



Object-oriented texture analysis for the unsupervised segmentation of biopsy images for cancer detection

Akif Burak Tosun^a, Melih Kandemir^a, Cenk Sokmensuer^b, Cigdem Gunduz-Demir^{a,*}

^aDepartment of Computer Engineering, Bilkent University, Ankara TR-06800, Turkey

^bDepartment of Pathology, Hacettepe University Medical School, Ankara TR-06100, Turkey

ARTICLE INFO

Article history:

Received 1 December 2007

Received in revised form 5 June 2008

Accepted 16 July 2008

Keywords:

Cancer detection

Image segmentation

Histopathological image analysis

Object-oriented texture

Colon adenocarcinoma

ABSTRACT

Staining methods routinely used in pathology lead to similar color distributions in the biologically different regions of histopathological images. This causes problems in image segmentation for the quantitative analysis and detection of cancer. To overcome this problem, unlike previous methods that use pixel distributions, we propose a new homogeneity measure based on the distribution of the objects that we define to represent tissue components. Using this measure, we demonstrate a new object-oriented segmentation algorithm. Working with colon biopsy images, we show that this algorithm segments the cancerous and normal regions with 94.89 percent accuracy on the average and significantly improves the segmentation accuracy compared to its pixel-based counterpart.

© 2008 Elsevier Ltd. All rights reserved.

1. Introduction

In the current practice of medicine, histopathological examination of biopsies is the most commonly used method to locate and classify diseases including cancer. In cancer diagnosis, pathologists visually examine the changes in cell morphology and tissue distribution under a microscope and determine whether a biopsy contains any malignant (cancerous) region and, if so, the cancer type and its malignancy level (grade). However, as it mainly relies on the visual interpretation, this examination may lead to a considerable amount of subjectivity, especially in cancer grading [1,2]. To reduce this subjectivity, it has been proposed to use computational methods that rely on the quantification of a tissue by defining mathematical features [3–7]. Although the very first step in this quantification is the segmentation of a tissue image into homogeneous regions, these studies have not mainly focused on this problem and have extracted features from the tissue image assuming that it is homogeneous. Nevertheless, besides having many heterogeneous regions in a tissue image, the existence of such regions and their ratio help pathologists determine the cancer grade.

It has been proposed to segment an image into homogeneous regions by either connecting adjacent pixels or locating edges

according to a homogeneity measure. Numerous studies have defined the homogeneity based on the color information of pixels and/or the spatial relations between the colors (i.e., texture information of pixels) [8,9]. A large subset of them quantizes the pixels of an image into clusters using the color information alone and considers the connected pixels of the same cluster as a homogeneous region [10–15]. One common method to find such clusters is to employ the color histogram of the image. For example, Park et al. [11] perform morphological operators on the histogram, while Shafarenko et al. [12] apply the watershed algorithm to the histogram to detect the clusters. Besides employing the color histogram, different approaches (such as fuzzy [13,14] and genetic [15] approaches) are also used to obtain the clusters. Another subset of studies proposes to use spatial information of pixels in addition to their color information [16–19]. The color and the texture information could be used consecutively or together in segmentation. For example, the JSEG algorithm proposed by Deng and Manjunath [17] first uses pixel color information to quantize them into clusters, without considering their spatial relations. Following the quantization, they define a homogeneity criterion to quantify the texture of the color-quantized pixels. In contrast, in the algorithm proposed by Chen et al. [19], the texture is extracted from the gray-scale of the image and it is used together with the color information to obtain the overall segmentation. As they commonly result in oversegmentation, both of these approaches merge the segmented regions according to their color similarity. These previously proposed segmentation algorithms lead to promising results especially when there is a considerable amount of difference in the color distribution of adjacent regions. However,

* Corresponding author. Tel.: +90 312 290 3443; fax: +90 312 266 4047.

E-mail addresses: tosun@cs.bilkent.edu.tr (A.B. Tosun), melih@cs.bilkent.edu.tr (M. Kandemir), csokmens@hacettepe.edu.tr (C. Sokmensuer), gunduz@cs.bilkent.edu.tr (C. Gunduz-Demir).

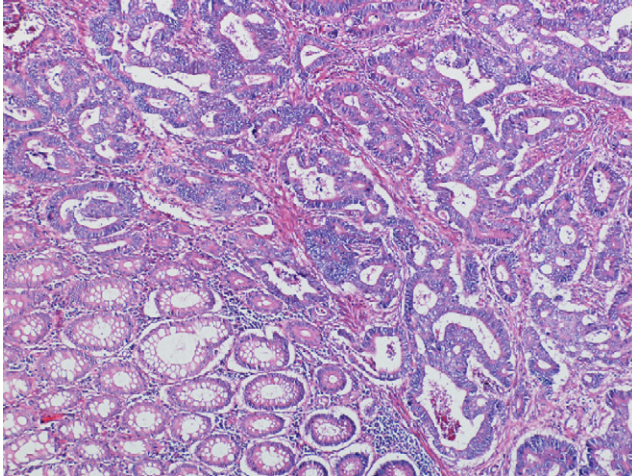


Fig. 1. A histopathological image stained with the hematoxylin-and-eosin technique.

due to the routinely used staining techniques, the color distribution of different regions is very similar for histopathological images. For instance, Fig. 1 shows such a histopathological image stained with the hematoxylin-and-eosin technique, which is routinely used to stain a biopsy in hospitals. As observed in this figure, this image consists of two regions in which the color distributions are very similar (here the upper right of the image contains tumorous regions whereas its lower left contains healthy regions).

In this paper, we introduce a new homogeneity measure and demonstrate a new segmentation algorithm that uses this homogeneity measure to segment a biopsy image, for which the color distribution is very similar in its heterogeneous regions. Our proposed approach relies on the quantification of the spatial relations between the tissue components (e.g., epithelial tissue components, connective tissue components, and luminal structures). For this purpose, we define different types of “objects”, which represent different components of a tissue, and make use of the distribution of these objects as well as their spatial relations to define our homogeneity measure. As opposed to the existing algorithms, which rely on pixel-based information (pixel colors and/or pixel-based textures), the proposed segmentation algorithm uses object-based information. Working with colon biopsy images, we demonstrate that our object-oriented segmentation algorithm yields 94.89 percent accuracy on the average and significantly improves the accuracy in locating tumorous regions and other non-cancerous tissue transformations compared to its pixel-based counterpart.

The remainder of this paper is organized as follows. In Section 2, we first provide our method to identify the objects in a tissue image, then describe our homogeneity criterion based on the spatial relations between the objects, and last explain our segmentation algorithm. Subsequently, we present our experiments and discuss their results in Section 3. Finally, we provide a summary of our work and discuss a future research perspective in Section 4.

2. Object-oriented textural segmentation

In a biopsy image, biologically different parts of the tissue are characterized with the spatial organizations of its cellular and connective tissue components. These organizations show differences, depending on the organ from which the tissue is taken. In this work, we focus on colon biopsy images where the tissue components are organized to form glandular structures. In these images, epithelial cells are lined up around a luminal structure, forming a crypt (gland), and lymphoid cells take place in between these crypts. This

organization deviates from its regular structure due to the existence of cancer. Furthermore, this deviation is aggravated with the increasing malignancy level. Thus, for the detection of cancer and its malignancy level, the regions containing such tumorous structures should be distinguished from those that contain the normal ones.

In this work, we propose a segmentation algorithm that uses the fact that the structural organization of a tissue (i.e., the spatial distributions of cellular and connective tissue components with respect to each other) changes with the existence of cancer. To this end, we define our homogeneity measure based on the texture of these components. We define primitive objects to represent these components, instead of exactly identifying their locations, since this localization brings about a more difficult segmentation problem even for human experts.

2.1. Object definition

For defining objects, we first run the k-means algorithm on the color intensities of pixels and quantize the pixels into three clusters. These clusters correspond to purple regions (for epithelial and lymphoid cell components), pink regions (for connective tissue components), and white regions (for both luminal structures and connective tissue components¹). Subsequently, we locate circular primitives on the pixels of each cluster after eliminating small holes and regions in the cluster. Since there are different ways of locating circles on a group of pixels, we make use of a heuristic in which the circular components are iteratively located. For a given set of pixels $\mathcal{P} = \{x_i\}$, this algorithm works as follows:

Step 1: It assigns each particular pixel x_i to the largest possible circle that includes this particular pixel x_i and that is formed by only the pixels $x_j \in \mathcal{P}$.

Step 2: It forms connected components $\mathcal{C} = \{C_1, C_2, \dots, C_N\}$ from the pixels such that the connected component C_k consists of the pixels that are assigned to the circle k . In this step, it also eliminates the connected components smaller than an area threshold.

Step 3: For each component C_k , it recursively calls Steps 1 and 2 considering only the pixels of this connected component (i.e., in Step 1, \mathcal{P} will be a set of pixels belonging to the component C_k) until there is no change in the pixels of the component. Note that there will be no change when a component is circular.

In our work, we run this iterative algorithm twice for each cluster. In the first run, we consider all of the pixels of the cluster and find the circular primitives. Then in the second run, we consider all of the pixels that belong to the same cluster but not belong to any of the circles found in the first run. Finally, the primitives obtained from the first and the second runs are merged. In Fig. 2, the results of iterations in the first and the second runs along with the final result are shown on a small image.

After this two-step iterative algorithm, we group the circular primitives of each cluster into two object types depending on their sizes. Here the circular primitives with a size smaller than a threshold are defined as one type of the object and those with a size greater than the threshold are defined as the other type. Therefore, at the end of this step, six different object types (depending on both the size of a primitive and the cluster that it belongs to) are defined for the tissue components of a given image. In Fig. 3(b), the object-map for

¹ Here “connective tissue components” is used as a general term, which represents the other components rather than cell nuclei and luminal structures. Pink-like color usually corresponds to the components such as cytoplasm, muscularis mucosa, and cell plate whereas white-like color usually corresponds to postfixative artificial defects in the connective tissue and materials secreted by neoplastic cells such as mucin.

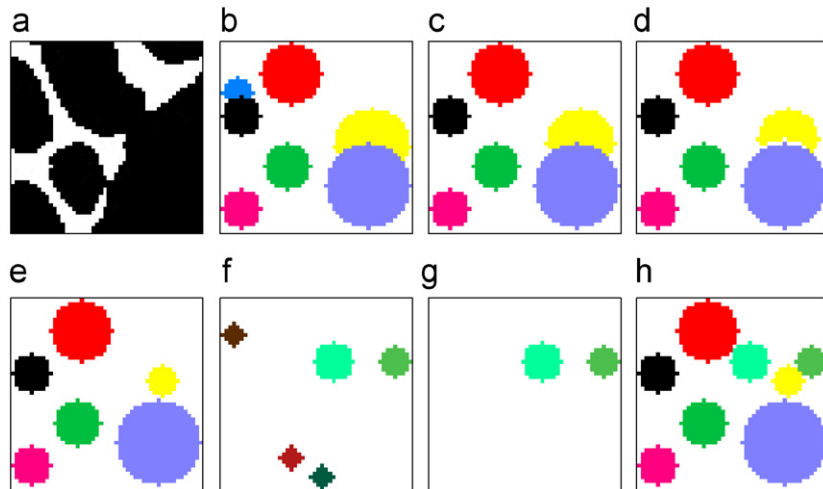


Fig. 2. The steps for locating circular primitives for a cluster: (a) pixels that belong to the cluster are shown with black; (b–e) the results of each iteration in the first run; (f,g) the results of each iteration in the second run; (h) final result obtained by merging the results of the first and the second runs.

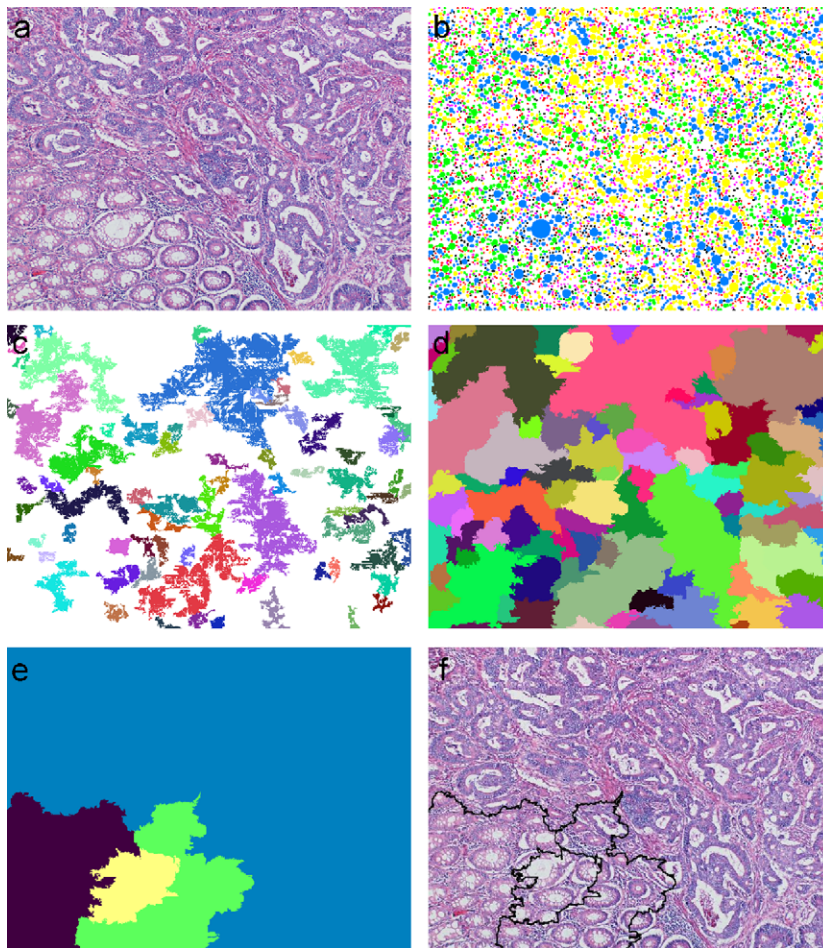


Fig. 3. The steps for the object-oriented segmentation of a biopsy image: (a) start with the original tissue image; (b) locate the circular objects on the quantized image; (c) determine the seeds; (d) grow the seeds; (e) merge the regions; and (f) the segmented image.

an exemplary tissue image (Fig. 3(a)) is illustrated. The motivation to define two different object types for the same cluster relies on the fact that each cluster may represent more than one tissue component. For example, purple cluster represents both the epithelial and

lymphoid cell components; epithelial cells are lined up around a luminal structure, forming a crypt, and lymphoid cells reside between these crypts. Since lymphoid cells are smaller and farther apart from each other compared to epithelial cells, these cells are expected to

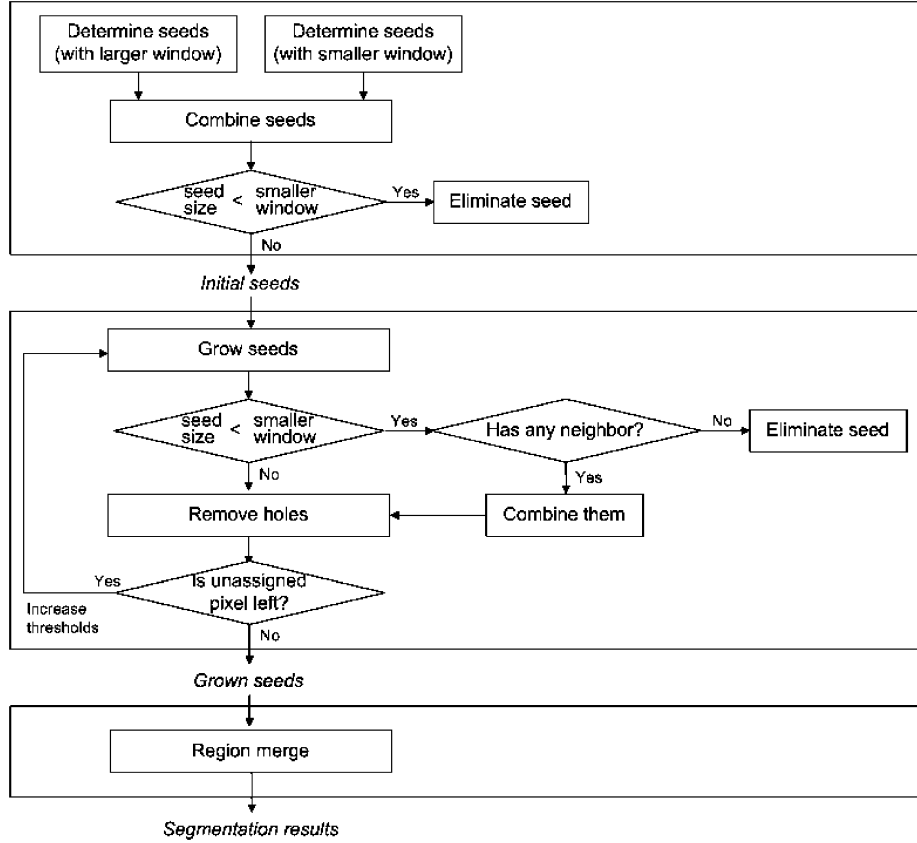


Fig. 4. A schematic of the proposed region-growing method.

form smaller circles. The definition of two different object types for the purple cluster could be helpful to represent this difference.²

2.2. Object-oriented texture definition

In our segmentation algorithm, we make use of the textural composition of the objects that we define for the representation of the tissue components. For this purpose, we propose a homogeneity criterion based on how the objects are distributed in size and in space. In a homogeneous image, for each object, there should be another one with the same object type and in its symmetric location. Also for each object type, the size of the objects should be the same. Thus, we define two measures:

- (1) *Object size uniformity*: It measures the uniformity in the object size. For this reason, for each particular object type, we use the standard deviation of the areas of the objects that belong to this particular object type. If the objects are uniformly distributed in size, the standard deviation of their areas should be equal to zero. Note that here we use the coefficient of variation since the different types of objects have areas of different scales.
- (2) *Object spatial distribution uniformity*: It quantifies how uniform the objects are distributed in space. For this purpose, for each particular object type, we compute the sum of the position vectors of every object, which belongs to this particular object type, with reference to the image centroid and use the magnitude

of the resulting vector. If the objects are uniformly distributed in space, the magnitude should be equal to zero. We define this measure particularly for the objects rather than the pixels, as opposed to the previous work of Deng and Manjunath [17] where this measure is strictly defined on the individual pixels. For this measure, instead of pixels, using objects overcomes the problem of dealing with images that exhibit similar color distributions in their different regions, unlike the previous literature.

2.3. Segmentation algorithm

In our segmentation algorithm, we propose to segment an image into regions for which the aforementioned two measures (object size uniformity and object spatial distribution uniformity) are minimized for all object types. As it is not feasible to minimize these measures for the entire image, we compute them over small windows and use them in our region-growing method. For this reason, we compute these measures using a window centered at each pixel in the image. Thus, for each pixel, there are a total of 12 uniformity measures, two measures for each of the six objects that we define for the representation of tissue components (Section 2.1).

Our region-growing method is a three-step procedure. In the first step, we determine the initial seeds based on the uniformity measures of pixels. In the second step, we iteratively grow these initial seeds also based on the uniformity measures. In the third step, we merge the oversegmented regions employing the object distributions. Next, we explain these steps in detail; a schematic of the proposed region-growing method is provided in Fig. 4.

² Although this does not provide an exact classification of tissue components, it helps group the similar tissue components into a single object type.

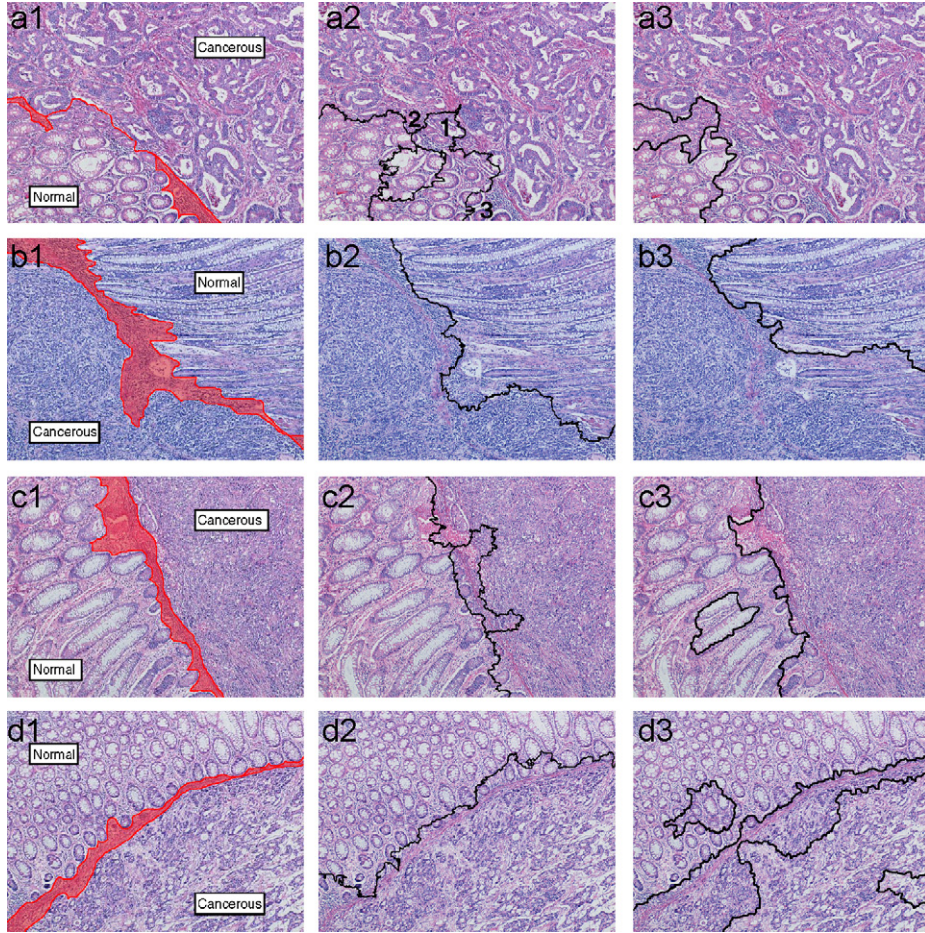


Fig. 5. The segmentation results. (a1)–(d1) The manual segmentations; (a2)–(d2) the results obtained by our object-based algorithm; (a3)–(d3) the results obtained by the JSEG algorithm.

2.3.1. Seed-determination

We determine the seeds by connecting pixels for which all of the 12 uniformity measures are smaller than their corresponding thresholds. In our algorithm, for each measure j , we set a threshold $T_j = \mu_j + \sigma_j$, where μ_j and σ_j are the mean and the standard deviation of the associated measure computed over all pixels. Note that here we connect the pixels based on the four-connectivity.

In addition to determining the seeds based on our uniformity measures computed within a particular window, we repeat the same procedure using a smaller window to capture finer textural information. Then, we combine the seeds obtained using both the larger and the smaller windows if their seeds do not overlap. In the case that these seeds overlap, we use the seeds obtained from the larger window and only the non-overlapping regions of the seeds obtained from the smaller window. At the end, we eliminate the seeds that are smaller than the size of the smaller window. Fig. 3(c) shows the seeds computed for the image given in Fig. 3(a).

2.3.2. Seed-growing

In the next step, we start growing the initial seeds using the same set of 12 uniformity measures. In the beginning, we compute the threshold values by considering the pixels that are not assigned to any of the seeds in the seed-determination step. Using the four-connectivity, we connect the unassigned pixels for which all of the measures are smaller than their corresponding thresholds to form a new connected component. If this new component is a neighbor

of a previously determined seed, we merge them together. In the case that this component has more than one neighbor, we merge it with its closest neighbor.³ If the component has no neighbors, then this component is considered as a new seed. We continue this iterative procedure for all of the remaining unassigned pixels until there is no unassigned pixel left with measures smaller than the thresholds. Note that, for each iteration, the threshold values are recomputed considering the mean and the standard deviation of only the remaining unassigned pixels from the previous iteration. After this iterative procedure is completed, if any of the determined seeds is smaller than the size of the smaller window, we connect it to its largest neighbor. In the case that it has no neighbors, we eliminate this seed. Finally, we fill in the holes of each seed.

We repeat this entire seed-growing procedure as necessary until there are no unassigned pixels left in the image. To do so, in its first iteration, we compute the threshold of the measures as $T_j = \mu_j + \sigma_j$ and update the threshold in the next iteration, by increasing the effect of σ_j incrementally each iteration. For the image given in Fig. 3(a), the final regions computed at the end of seed-growing step are shown in Fig. 3(d).

³ To select the closest neighbor, we compute the same measure set over the pixels of the component as well as over those of its neighbors. We compute the Euclidean distance between the measures of the component and those of each neighbor as the closeness measure.

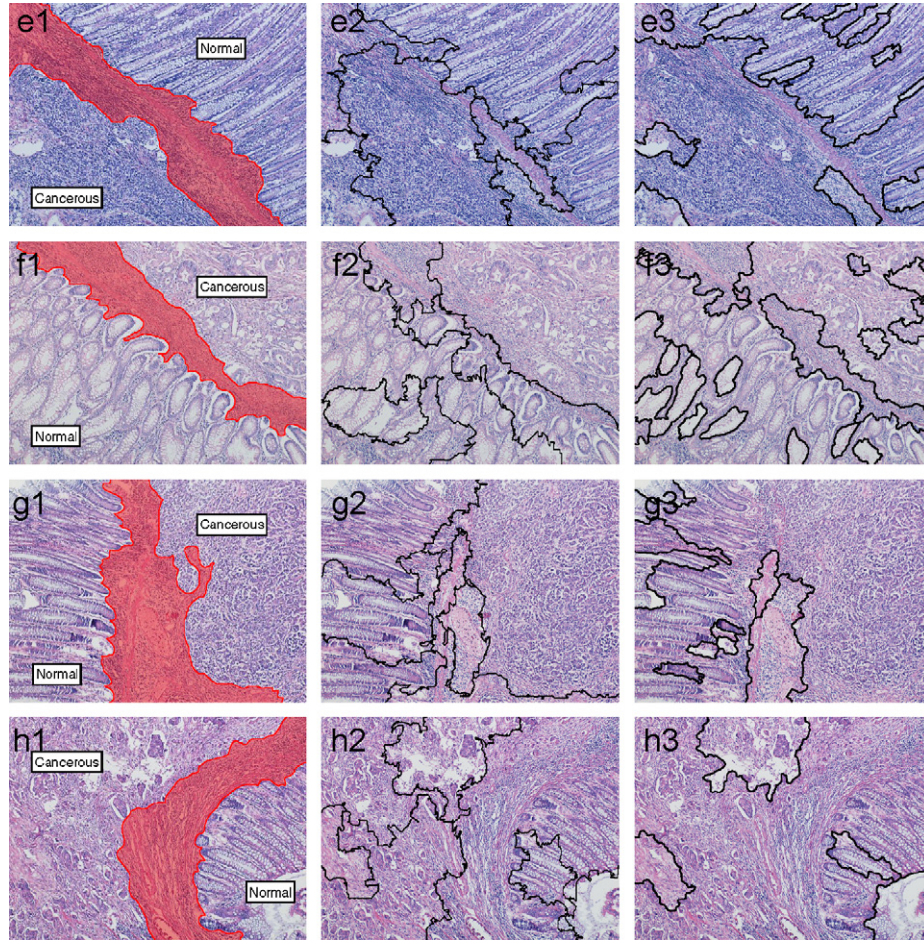


Fig. 6. The segmentation results. (e1)–(h1) The manual segmentations; (e2)–(h2) the results obtained by our object-based algorithm; (e3)–(h3) the results obtained by the JSEG algorithm.

2.3.3. Region-merge

The seed-growing step often results in oversegmented regions. For this reason, in the final step, we merge these regions based on their object distributions. In our region-merge step, we use two different criteria to characterize a region: (1) the percentage of the total area of the same type of objects in the region and (2) the percentage of the combined areas of the different objects that correspond to the same cluster in the region. Using these criteria, we first merge a region with its closest neighbor if its size is smaller than the larger window size. In the case that its size is larger, we only combine it with its closest neighbor only if the distance between them is smaller than the merge threshold. It is worth noting that after merging a region with its neighbor, we update the criteria accordingly and continue the merge with the updated criteria. For the image in Fig. 3(a), the regions obtained at the end of the region-merge step are illustrated in Fig. 3(e) and the final boundaries are superimposed on the original image in Fig. 3(f).

3. Experiments

3.1. Results

In our experiments, we use the microscopic images of colon biopsy samples of 16 randomly chosen patients from the Pathology Department archives in Hacettepe School of Medicine. Each biopsy sample consists of a 5–6 μm -thick tissue section stained with the hematoxylin-and-eosin technique. The images of these samples are

taken in the RGB color space using a Nikon Coolscope Digital Microscope; 5 \times microscope objective lens is used and the image resolution is 1920 \times 2560. Each colon biopsy image contains both normal and cancerous (colon adenocarcinomatous) regions. Cancerous regions contain tumors with different grades. In Figs. 5–8, the first image of each row consists of the manual segmentation provided by our medical expert.⁴ For each tissue image, the regions are labeled as either cancerous or normal and the boundary between these regions are drawn in red. In between these boundaries, there are also regions that can be included in either side without affecting the medical interpretation; such regions are shaded in red.

In Figs. 5–8, the second column of each row shows the segmentation results for each image that are obtained by our object-oriented segmentation algorithm. To compare our results with those obtained from a pixel-based segmentation algorithm, we also run the JSEG algorithm, which is proposed by Deng and Manjunath [17]. This algorithm separately uses the color information of pixels and their texture composition to segment an image into its homogeneous regions. In our experiments, we use the program provided by its authors in their web site.⁵ The results obtained by this program are also presented in the third columns of Figs. 5–8. For both our segmentation algorithm and the JSEG algorithm, the selection of

⁴ By Professor C. Sokmensuer, MD, who is specialized in colorectal carcinomas and has been practicing oncology for the last 15 years.

⁵ The program is available at <http://vision.ece.ucsb.edu/segmentation/jseg/software>.

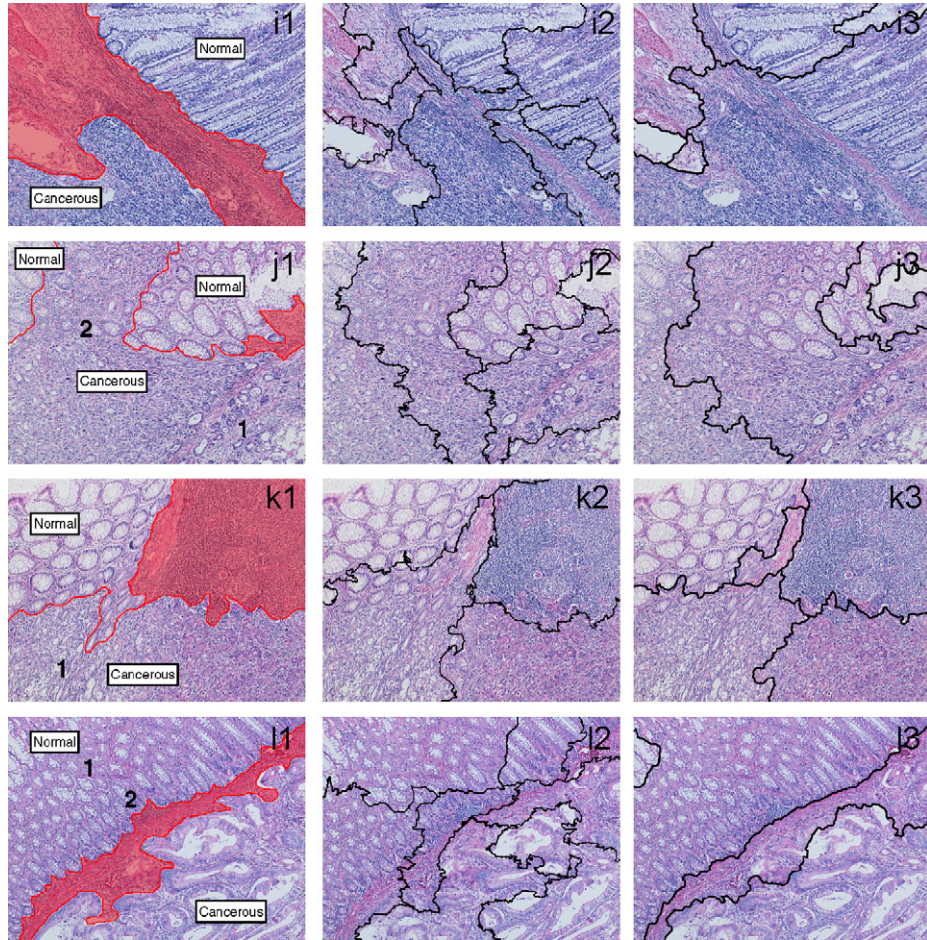


Fig. 7. The segmentation results. (i1)–(l1) The manual segmentations; (i2)–(l2) the results obtained by our object-based algorithm; (i3)–(l3) the results obtained by the JSEG algorithm.

the merge threshold parameter affects the results. In Figs. 5–8, we provide the results of each of these algorithms, selecting the best merge parameter for each image. Additionally, for the JSEG algorithm, we also select the best color quantization threshold and the best number of scales for each image.

In our algorithm, besides the merge parameter, we use the same set of parameters for all images. To define our circular primitives, we set the area threshold parameter to be 100 pixels so that it is large enough to eliminate the noise and small enough to represent the tissue components. Also in defining the objects from the circular primitives, we use an object area threshold of 150 pixels to accommodate different tissue components represented by the same cluster. In the seed-determination, we use the window sizes of 257 and 65 pixels for the large and small windows to determine sufficiently coarse and fine textures in our images with a resolution of 1920×2560 . In the region-growing step, we increment the effect of the standard deviation by 10 percent of its value in each iteration for computational reasons.

3.2. Discussion

For the colon biopsy image shown in Fig. 5(a), our object-based algorithm leads to accurate segmentation. It results in only one cancerous crypt (marked with 1) being included in the normal region and only a small amount of normal crypts (marked with 2 and 3)

being included to the cancerous region (Fig. 5(a2)). On the other hand, the pixel-based algorithm yields a segmented region for cancerous parts that contain a significant amount of normal crypts (Fig. 5(a3)). Similarly, for the image given in Fig. 5(b), our object-based segmentation algorithm yields accurate results and greatly improves the specificity and the accuracy compared to the pixel-based algorithm. Higher specificity (i.e., having less number of false positives) is important for correct grading of cancer. In cancer grading, the grade measures how much a tissue differentiates from the normal. The correct grading of cancer is critical since it affects the selection of the treatment and is an important predictor for the survival time of a patient. In colon adenocarcinoma grading, the differentiation is quantified according to how much the glands of a cancerous region are similar to the normal gland. False positives affect this quantification and cause to select a lower grade.

For the images given in Fig. 5(c) and (d), both the pixel-based and the object-based algorithms yield accurate results in the segmentation of their adenocarcinomatous and normal regions.

For the images given in Figs. 6(e)–(g), both of the algorithms result in oversegmentation. However, although the object-based segmentation algorithm does not have a heterogeneous region, which includes both cancerous and normal parts, the pixel-based segmentation algorithm has one that contains both of these parts. Similarly, for Figs. 6(h) and 7(i), the pixel-based algorithm leads to heterogeneous regions, and thus, yields lower segmentation accuracy compared to the object-based algorithm.

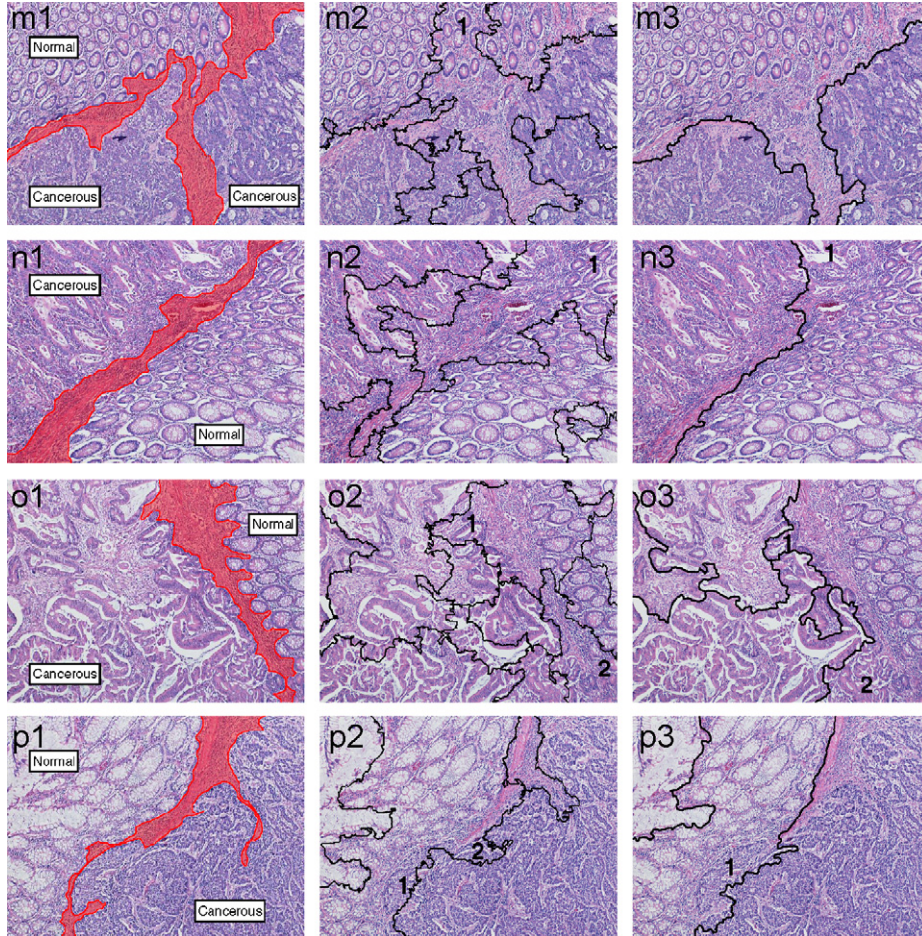


Fig. 8. The segmentation results. (m1)–(p1) The manual segmentations; (m2)–(p2) the results obtained by our object-based algorithm; (m3)–(p3) the results obtained by the JSEG algorithm.

In Figs. 7(j) and (k), there are heterogeneity in the tumor such that it contains regions of both grade 2 (marked with 1) and grade 3 (cancerous regions other than that marked with 1). Besides, in Fig. 7(j), in the regions marked with 2, the tumor infiltrates into normal regions. For this image, our object-based algorithm successfully segments the normal region that is located in the upper left from the cancerous parts and captures the heterogeneity in cancerous regions. On the other hand, although the pixel-based algorithm identifies some part of this normal region, it could not capture the heterogeneity in the tumor. For this image, neither the object-based nor the pixel-based algorithms can segment the normal crypts that are in the top right of the image. For the image given in Fig. 7(k), both the pixel-based and the object-based algorithms capture the heterogeneity in the tumor. For the image shown in Fig. 7(l), both of the algorithms segment the normal and cancerous regions with an acceptable accuracy. At a first glance, it could be considered that the pixel-based algorithm yields better results since the object-based algorithm results in oversegmentation. However, when the normal regions are examined carefully, it is observed that normal regions contain some non-tumorous transformations (oncocytic and hyperplastic transformations) as well as lymphoid aggregations (regions marked with 1 and 2, respectively). Although the pixel-based algorithm does not capture these transformations, the object-based algorithm is successful to do that and distinguish the regions containing such transformations from those that do not contain any. The identification of such heterogeneities is important for cancer grading and

prognosis. The heterogeneity in the tumor is known to affect the cancer grade, while non-cancerous tissue transformations are presently believed to be the prognostic parameters, which is further expected to be better understood in the future.

For the image shown in Fig. 8(m), the object-based algorithm incorrectly segments a normal region (marked with 1 in Fig. 8(m2)) and oversegments the remaining cancerous regions. For this image, the pixel-based approach achieves a successful segmentation.

For the image given in Fig. 8(n), both the pixel-based and the object-based algorithms lead to a heterogeneous region, which contains both normal and cancerous parts (regions marked with 1 in Figs. 8(n2) and (n3)). Besides this heterogeneous region, our segmentation algorithm results in more number of segmented regions compared to the pixel-based algorithm; this is attributed to the prominent lymphoid reaction in the tumor. Similarly, for the images given in Figs. 8(o) and (p), both of the algorithms result in heterogeneous regions (regions marked with 1 and 2 in Figs. 8(o2), (o3), (p2), and (p3)). In spite of these heterogeneous regions, both of the algorithm yield acceptable accuracies for all these images.

In order to quantitatively compare the segmentation results of the object-based and the pixel-based algorithms, we calculate the true positive, false positive, true negative, and false negative rates using the manual segmentation as the gold standard and then report the sensitivity, specificity, and accuracy of these algorithms. Since both our object-oriented algorithm and the JSEG algorithm are unsupervised segmentation methods, they do not output the class of

Table 1

The average and the standard deviation of the sensitivity, specificity, and accuracy percentages for the object-based and the pixel-based algorithms

	Object-based	Pixel-based
Sensitivity	96.05 ± 5.72	86.25 ± 31.32
Specificity	92.22 ± 10.56	78.27 ± 26.38
Accuracy	94.89 ± 3.77	86.78 ± 11.46

the segmented regions. Therefore, we consider the class of the dominant region as the label of the region and calculate the true positive, false positive, true negative, and false negative rates accordingly. In our calculation, we do not consider the pixels that could be included in either side (either cancerous or normal region) without affecting the medical interpretation (the pixels that are shaded in red in Figs. 5–8). We report the average and the standard deviation of the sensitivity, specificity, and accuracy percentages in Table 1. This table shows that our object-oriented algorithm yields higher sensitivity and specificity percentages and that it improves the accuracy of the JSEG algorithm for the segmentation of histopathological images. To investigate whether or not this improvement is significant, we use the Wilcoxon test with a significance level of 0.05. This test exhibits that this improvement is statistically significant.

4. Conclusion

In this work, we proposed a new homogeneity measure based on the distribution of the objects. For this purpose, we defined objects to represent tissue components including epithelial tissue components, connective tissue components, and luminal structures. Using this object-oriented measure, we demonstrated a new object-based segmentation algorithm. As opposed to the existing algorithms that use pixel-based information in defining their homogeneity measure, our segmentation algorithm uses object-based information, for the first time.

Working with colon biopsy images with similar color distributions in their heterogeneous regions, we demonstrate that our object-oriented algorithm significantly improves the accuracy in segmenting tumorous regions and also other non-cancerous tissue transformations compared to its pixel-based counterpart. Our future research directions include examining the use of supervised classification algorithms in merging the segmented regions and extracting a set of quantitative features from the segmented regions for cancer grading.

About the Author—AKIF BURAK TOSUN received his B.Sc. degree in computer engineering from Hacettepe University, Turkey, in 2006, and is currently working toward his Ph.D. degree in computer engineering at Bilkent University, Turkey. His research work includes the development of novel image segmentation approaches for cancer diagnosis under the supervision of Dr. Gunduz-Demir at Bilkent University.

About the Author—MELIH KANDEMIR received his B.Sc. degree in computer engineering from Hacettepe University, Turkey, in 2005, and is presently in M.S. program in computer engineering at Bilkent University, Turkey. His research work includes implementation and comparison of different segmentation tools under the supervision of Dr. Gunduz-Demir at Bilkent University.

About the Author—CENK SOKMENSUER received his medical degree and his pathology training from Hacettepe University, School of Medicine, Turkey, and currently holds the rank of Professor of Pathology at Hacettepe University. As a visiting scholar, he worked in Harvard University in the USA in 2003–2004, in Necker Children Hospital in France in 1998, and in Victor Dupuy Hospital in France in 1992. His specialization includes pathology of gastrointestinal system, liver, and endocrine system.

About the Author—CIGDEM GUNDUZ-DEMIR received her B.S. and M.S. degrees in computer engineering from Bogazici University, Turkey, in 1999 and 2001, respectively, and Ph.D. degree in computer science from Rensselaer Polytechnic Institute, New York, in 2005. She joined Bilkent University in 2006, where she is currently Assistant Professor at the Department of Computer Engineering. Her research interests include the construction of new bio-computational models and application of computer vision and machine learning algorithms for diagnostic and prognostic purposes in cancer research, in particular, and in medicine, in general. She is the recipient of CAREER Award of the National Scientific and Technological Research Council of Turkey.

Acknowledgments

This work has been supported by the Scientific and Technological Research Council of Turkey under the Project no. TÜBİTAK 106E118.

References

- [1] A. Andriom, C. Magnani, P.G. Betta, A. Donna, F. Mollo, M. Scelsi, P. Bernardi, M. Botta, B. Terracini, Malignant mesothelioma of the pleura: interobserver variability, *J. Clin. Pathol.* 48 (1995) 856–860.
- [2] G.D. Thomas, M.F. Dixon, N.C. Smeeton, N.S. Williams, Observer variation in the histological grading of rectal carcinoma, *J. Clin. Pathol.* 36 (1983) 385–391.
- [3] P.W. Hamilton, P.H. Bartels, D. Thompson, N.H. Anderson, R. Montironi, Automated location of dysplastic fields in colorectal histology using image texture analysis, *J. Pathol.* 182 (1997) 68–75.
- [4] S.J. Keenan, J. Diamond, W.G. McCluggage, H. Bharucha, D. Thompson, B.H. Bartels, P.W. Hamilton, An automated machine vision system for the histological grading of cervical intraepithelial neoplasia (CIN), *J. Pathol.* 192 (2000) 351–362.
- [5] A.N. Esgiar, R.N.G. Naguib, B.S. Sharif, M.K. Bennett, A. Murray, Fractal analysis in the detection of colonic cancer images, *IEEE Trans. Inf. Technol. Biomed.* 6 (2002) 54–58.
- [6] C. Demir, S.H. Gultekin, B. Yener, Learning the topological properties of brain tumors, *IEEE-ACM Trans. Comput. Biol. Bioinformatics* 2 (3) (2005) 262–270.
- [7] C. Demir, S.H. Gultekin, B. Yener, Augmented cell-graphs for automated cancer diagnosis, *Bioinformatics* 21 (Suppl. 2) (2005) i17–i12.
- [8] L. Lucchese, S.K. Mitra, Color image segmentation: a state-of-the-art survey, image processing, vision, and pattern recognition, in: Proceedings of the Indian National Science Academy, New Delhi, India, vol. 67A, No. 2, 2001, pp. 207–221.
- [9] D.L. Pham, C. Xu, J.L. Prince, Current methods in medical image segmentation, *Annu. Rev. Biomed. Eng.* 2 (2000) 315–338.
- [10] Y.I. Ohta, T. Kanade, T. Sakai, Color information for region segmentation, *Comput. Vision, Graphics, Image Process.* 13 (1980) 222–241.
- [11] S.H. Park, I.D. Yun, S.U. Lee, Color image segmentation based on 3D clustering-morphological approach, *Pattern Recognition* 31 (8) (1998) 1061–1076.
- [12] L. Shafarenko, M. Petrou, J.V. Kittler, Histogram based segmentation in a perceptually uniform color space, *IEEE Trans. Image Process.* 7 (9) (1998) 1354–1358.
- [13] T.Q. Chen, Y. Lu, Color image segmentation: an innovative approach, *Pattern Recognition* 35 (2) (2002) 395–405.
- [14] T. Huntsberger, C. Jacobs, R. Cannon, Iterative fuzzy image segmentation, *Pattern Recognition* 18 (2) (1985) 131–138.
- [15] P. Scheunders, A genetic c-means clustering algorithm applied to color image quantization, *Pattern Recognition* 30 (6) (1997) 859–866.
- [16] H. Cheng, X. Jiang, J. Wang, Color image segmentation based on homogram thresholding and region merging, *Pattern Recognition* 35 (2) (2002) 373–393.
- [17] Y. Deng, B.S. Manjunath, Unsupervised segmentation of color-texture regions in images and video, *IEEE Trans. Pattern Anal. Mach. Learn.* 23 (8) (2001) 800–810.
- [18] F. Jing, M. Li, H.J. Zhang, B. Zhang, Unsupervised image segmentation using local homogeneity analysis, in: Proceedings of the 2003 International Symposium on Circuits and Systems, vol. 2, 2003, pp. II-456–II-459.
- [19] J. Chen, T.N. Pappas, A. Mojsilovic, B.E. Rogowitz, Adaptive perceptual color-texture image segmentation, *IEEE Trans. Image Process.* 14 (10) (2005) 1524–1536.